

Origins, Structure, and Inflows of $m = 1$ Modes in Quasi-Keplerian Disks

Philip F. Hopkins^{1*}

¹*Department of Astronomy, University of California Berkeley, Berkeley, CA 94720*

Submitted to MNRAS, September, 2010

ABSTRACT

Simulations show eccentric disks ($m = 1$ modes) forming around quasi-Keplerian potentials, a topic of interest for fueling quasars, forming super-massive BHs, planet formation and migration, explaining the origin and properties of nuclear eccentric stellar disks like that in M31, and driving the formation of the obscuring AGN torus. We consider the global, linear normal $m = 1$ modes in collisionless disks, without the restriction that the disk mass be negligible relative to the central (Keplerian) mass. We derive their structure and key resonance features, and show how they arise, propagate inwards, and drive both inflow/outflow and eccentricities in the disk. We compare with hydrodynamic simulations of such disks around a super-massive BH, with star formation, gas cooling, and feedback. We derive the dependence of the normal mode structure on disk structure, mass profiles, and thickness, and mode pattern speeds and growth rates. We show that, if the disk at some radii has mass of $\gtrsim 10\%$ the central point mass, the modes are linearly unstable and are self-generating. They arise as “fast modes” with pattern speed of order the local angular velocity at these radii. The characteristic global normal modes have pattern speeds comparable to the linear growth rate, of order $(GM_0 R_0^{-3})^{1/2}$, where M_0 is the central mass and R_0 is the radius where the enclosed disk mass $\sim M_0$. They propagate inwards by exciting eccentricities towards smaller and smaller radii, until at small radii these are “slow modes.” With moderate amplitude, the global normal modes can lead to shocks and significant gas inflows at near-Eddington rates at all radii inside several $\sim R_0$.

Key words: quasars: general — galaxies: active — galaxies: evolution — galaxies: nuclei — cosmology: theory

1 INTRODUCTION

Perturbations to normally circular orbits in nearly-Keplerian potentials are of fundamental interest for a variety of topics in astrophysics. For example, questions related to the fueling of super-massive black holes (BHs), their accretion disks, and the dynamics of nearby systems, the formation and fueling of protostars, and the behavior of protoplanetary disks and planets around stars or rings and moons around planets. Particularly interesting are perturbations with azimuthal wavenumber $m = 1$ (amplitude $\propto \cos \phi$), which can manifest as eccentric orbits or disks, lopsided or sloshing modes, or one-armed spirals. It is easy to see why: the response of a nearly circular orbit to a weak perturbation, to leading order, scales with $1/[\kappa^2 - m(\Omega - \Omega_p)^2]$, where Ω is the orbital frequency, κ is the epicyclic frequency, and Ω_p is the characteristic frequency (precession rate) of the perturbation. In a Keplerian potential, $\kappa = \Omega \propto r^{-3/2}$, so (since Ω_p is finite) for any continuous system this scales at small radii as $\sim 1/(1 - m)\Omega^2$. For general m ,

this vanishes, but for $m = 1$ the leading terms cancel and there is a strong resonant response. Physically, this 1:1 resonance between radial and azimuthal frequencies is related to the fact that elliptical orbits in a Keplerian potential are closed and do not precess. As a consequence, the eccentricity distribution and mode behavior in such a disk can be determined by collective effects in the disk, even where these collective effects are very weak compared to the gravity of the central object.

Recently, for example, Hopkins & Quataert (2009) have shown that the formation of lopsided, eccentric disks within the BH radius of influence is a ubiquitous feature in hydrodynamic simulations of massive gas inflows in galaxies, and that such disks can efficiently drive gas angular momentum loss and power BH accretion rates of up to $\sim 10 M_\odot \text{ yr}^{-1}$. The co-existence of gas and stars is critical for the large inflow rates seen; the torques on the gas are dominated by the mode in the collisionless portion of the disk. And the stellar relics of these disks bear a remarkable similarity to nuclear disks observed on $\lesssim 10 \text{ pc}$ scales around nearby supermassive BHs, particularly the well-studied case at the center of M31 (Lauer et al. 1993), whose origin has been mysterious. The inflow and out-

* E-mail: phopkins@astro.berkeley.edu

flow regulated by these modes in such simulations also determines the nature of the galaxy mass profile on scales within $\lesssim 10 - 100$ pc. As such, it is also particularly interesting to understand whether or not such modes could arise generically. There are many candidate nuclear disks in such systems (Lauer et al. 1996, 2005; Houghton et al. 2006; Thatte et al. 2000; Debattista et al. 2006; Afanasiev & Sil'chenko 2002; Seth et al. 2010).

There is considerable literature discussing the mode structure, pattern speeds, and evolution of general self-gravitating disk instabilities (see e.g. Lin et al. 1969; Goldreich & Tremaine 1978, 1979; Toomre 1969, 1977). But these $m = 1$ modes are less well-understood, especially in collisionless (stellar or planetary) disks. For example, there remains considerable debate regarding the stability of such modes (e.g. Tremaine 2001; Salow & Statler 2001; Jacobs & Sellwood 2001; Touma 2002). These works describe many interesting behaviors of $m = 1$ modes in a disk in a nearly Keplerian potential, but their conclusions rely on specific assumptions. Tremaine (2001) show that such modes are linearly stable, but only in the limit where $M_d \ll M_{\text{BH}}$ at all radii. And much of the insight from the study of protostellar and planetary disks focuses on either the same limit (for planetary disks) or the opposite limit (for early-stage protostellar disks) in which the system is really just a self-gravitating disk (see Laughlin & Bodenheimer 1994; Laughlin & Rozyczka 1996, and references therein). But in simulations or observations of galactic nuclei (Levine et al. 2008; Escala 2007; Mayer et al. 2007; Hopkins et al. 2010; Hopkins & Quataert 2009) and protostellar evolution (Laughlin & Bodenheimer 1994; Bate et al. 1995; Nelson et al. 1998), much of the interesting behavior involves disks over a range of radii where the disk is not completely negligible in mass. The mode structure outlined in Tremaine (2001) is used in Papaloizou (2002) to estimate the effects on a one or two low-mass planet system, but assuming mode stability and under similar mass and radius restrictions (and not allowing for a large collisionless disk component). Adams et al. (1989) and Ostriker et al. (1992); Shu et al. (1990) reach opposite conclusions to Tremaine (2001), but they focus on “fast modes” ($\Omega_p \sim \Omega$) in the regime $M_d \sim M_{\text{BH}}$ (or $M_d \sim M_*$), and consider only pure fluid disks with a hard and reflecting outer edge, in which case the resulting mode growth rates depend sensitively on the structure and nature of reflection at the disk edge (and can be dramatically modified – in fact, completely eliminated – allowing any flow “through” or outside the edge, the most probable configuration). In general, collisionless disks can have very different mode structure from fluid systems. Christodoulou & Narayan (1992) consider instabilities of narrow torus annuli (as opposed to disks) but with similar restrictions. Also, because the mode growth is sensitive to motion of the center of mass, most numerical studies to date have lacked the resolution to determine whether mode growth is real or artificial in the limit where the disk mass is smaller than the BH/star mass (see the discussion in Nelson et al. 1998).

Moreover, these studies have largely been restricted to very specific mass profiles (e.g. the Kuz'min disk, with $\Sigma \rightarrow \text{constant}$ at small radii) and/or systems with sharp “edges,” where in fact the profiles seen in interesting phases in simulations and in e.g. star-forming systems and the centers of real “cusp” elliptical galaxies resemble a range of power-law slopes with smooth declines at large radii and significant variation in profile shape (Gebhardt et al. 1996; Hopkins et al. 2009; Hopkins & Hernquist 2010).

As such, the origin of these modes, where observed, and many of their properties have remained ambiguous. Given claims of the stability of such modes, alternative suggestions for their origin have ranged from their being induced by an external collision/passage

(in galactic nuclei, from e.g. a nuclear star cluster; see Sambhus & Sridhar 2002), to their being excited by substantial populations of stars on retrograde orbits (Touma 2002). But these explanations pertain only to very specific systems or regimes, and do not explain the ubiquity of such modes in astrophysical systems. Showing that they can in fact be self-generating via gravitational instability would have profound implications.

Moreover, in systems with star or planet formation as an ongoing process, these modes will evolve in time, as quantities such as the disk gas fraction, mass profile, dispersion profile, and total disk mass are affected by these processes. Similarly, the modes in the collisionless disk can drive very strong inflows and outflows in gas, changing the properties of the host disks in turn (see Nelson et al. 1998; Bounaud et al. 2005; Hopkins & Quataert 2009). Therefore it is of great importance to both survey a range of analytic profile shapes and dispersion levels, and to compare with simulations that can incorporate non-linear effects on the mode evolution. It is also particularly interesting to examine the level of inflow generated by such modes, if the disks have some gas.

In this paper we expand upon the investigation of global $m = 1$ modes in nearly Keplerian, predominantly collisionless disks. In particular, we focus on the question of whether or not such modes can, in fact, be unstable and self-generating, and if so how they propagate throughout such disks. After defining some terms (§ 2), we consider modes in the local (WKB) limit (§ 3), which allows us to analytically derive approximate stability criteria and discuss conditions for efficient mode propagation, in both gaseous and stellar disks. In § 4, we discuss exact numerical solutions which allow us to extend this discussion to linear global normal modes, and outline under what conditions these modes are unstable (and what their characteristic frequencies are), and how this depends on a variety of disk properties including mass profile shape, mass, and disk thickness. We discuss the structure of such modes, and the conditions under which they will drive shocks in collisionless+gaseous systems and corresponding inflow/outflow, and the radii over which the modes can act. In § 5, we compare to the results from high-resolution hydrodynamic simulations which include self-gravity, gas cooling, star formation, shocks, inflow/outflow, and non-linear effects all not captured in an analytic formulation, and discuss how this compares to our analytic insight. Finally, in § 6, we summarize our conclusions and their implications for astrophysical systems.

2 DEFINITIONS

Adopt a cylindrical coordinate frame, (R, ϕ, z) , and consider an initially axisymmetric, thin, planar disk with an arbitrary spherical (BH+bulge+halo) component. The coordinate center is located at the BH.

The initial potential in the disk plane can be written $\Phi_0 = \Phi_0(R)$, and other properties are defined in standard terms:

$$\Phi_0 = \Phi_0(R) \quad (1)$$

$$V_c^2 = R \frac{\partial \Phi}{\partial R} \approx \frac{GM_{\text{enc}}(< R)}{R} \quad (2)$$

$$\Omega \equiv t_{\text{dyn}}^{-1} = V_c / R \quad (3)$$

$$\kappa^2 \equiv R \frac{d\Omega^2}{dR} + 4\Omega^2 = \frac{\partial^2 \Phi}{\partial R^2} + 3\Omega^2 \quad (4)$$

where V_c is the circular velocity, Ω the angular velocity, and κ the epicyclic frequency. We use c_s to denote the sound speed in a gaseous disk and σ_z the vertical dispersion in a stellar disk.

Consider a perturbation in the plane and define the perturbed surface density field by

$$\Sigma \rightarrow \Sigma_0(R) + \Sigma_1(R, \phi) \quad (5)$$

We consider a frame rotating with the perturbation pattern speed Ω_p . We can represent the perturbed system as a sum of linearly independent modes m , $\Sigma_1 \equiv \sum_{m=1}^{\infty} \Sigma_m$. Since we will focus on the behavior of these modes individually, consider (without loss of generality), the case of a single mode,

$$\Sigma_m \equiv \Sigma_a(R) \exp \{i(m\phi - \omega t)\} \quad (6)$$

$$\Sigma_a(R) \equiv |a(R)| \Sigma_0(R) \exp \left\{ i \int^R k dR \right\} \quad (7)$$

where m is the azimuthal wavenumber, $|a| = |a(R)|$ the effective mode amplitude, k the radial wavenumber, and the complex ω the mode frequency. With these definitions, the mode pattern speed is $\Omega_p \equiv \text{Re}(\omega)/m$, and the linear mode growth rate is $\gamma \equiv \text{Im}(\omega)$ ($|a| \propto \exp(+\gamma t)$).

The mode of particular interest is an $m = 1$ mode, in a quasi-Keplerian potential. Simulations in which these inflows form self-consistently, including gas inflow, star formation, and feedback, typically find that the nuclear stellar and gas distributions are well-approximated by power laws on the scales of interest (Hopkins & Quataert 2009). We will therefore adopt a true power-law disk as a convenient reference model. For such a disk

$$\Sigma \propto R^{-\eta} = \Sigma_0 \left(\frac{R}{R_0} \right)^{-\eta} \quad (8)$$

and it is straightforward to show that

$$V_c^2 = 2\pi \alpha G \Sigma R \quad (9)$$

$$M_d(< R) = 2\pi (2 - \eta)^{-1} \Sigma R^2 \quad (10)$$

$$\alpha = \frac{\Gamma[1 - \frac{\eta}{2}] \Gamma[\frac{1+\eta}{2}]}{\Gamma[\frac{3-\eta}{2}] \Gamma[\frac{\eta}{2}]} \quad (11)$$

for $0 < \eta < 2$ ($\alpha \approx \eta$ for $\eta \leq 1$, $\approx 1/(2 - \eta)$ for $1 \leq \eta < 2$). Around a central BH this gives

$$\Omega^2 = \frac{GM_{\text{BH}}}{r^3} + \frac{2\pi \alpha G \Sigma_0}{R_0} \left(\frac{R}{R_0} \right)^{-(\eta+1)} \quad (12)$$

$$\kappa^2 = \frac{GM_{\text{BH}}}{r^3} + (3 - \eta) \frac{2\pi \alpha G \Sigma_0}{R_0} \left(\frac{R}{R_0} \right)^{-(\eta+1)}. \quad (13)$$

We will also discuss finite disks, with a power-law cutoff (motivated by analogy to the Kuz'min disk) of the form

$$\Sigma = \Sigma_0 \left(\frac{R}{R_0} \right)^{-\eta} \left[1 + \left(\frac{R}{a} \right)^2 \right]^{-(3-\eta)/2} \quad (14)$$

so that $\Sigma \propto R^{-\eta}$ at small radii and $\Sigma \propto R^{-3}$ at large radii. The total mass in the disk is then

$$M_d = \Sigma_0 a^2 \left(\frac{a}{R_0} \right)^{-\eta} \frac{\pi^{3/2} \Gamma[1 - \eta/2]}{\Gamma[(3 - \eta)/2]}. \quad (15)$$

In this case, Ω (and the potential) must be evaluated numerically, but for purposes of interpretation, they can be approximated well (exactly at small/large R and with $\sim 10\%$ accuracy at $R \sim a$) by

$$\Omega^2 \approx \frac{GM_{\text{BH}}}{r^3} + \frac{2\pi \alpha G \Sigma_0}{R_0} \left(\frac{R}{R_0} \right)^{-(\eta+1)} \left[1 + \mu \left(\frac{R}{a} \right)^2 \right]^{-1+\eta/2} \quad (16)$$

where $\mu^{-(2-\eta)/2} \equiv (\pi^{1/2} \Gamma[1 - \eta/2]) / (2\alpha \Gamma[(3 - \eta)/2])$. At small

radii this is just the normal power-law disk Ω , at large radii the disk portion simply becomes Keplerian, $\Omega^2 \rightarrow G(M_{\text{BH}} + M_d)/r^3$.

Although we, for convenience, define our canonical model with respect to a super-massive BH, many of our conclusions could identically be applied to *any* sufficiently collisionless disk in a quasi-Keplerian potential (e.g. protostellar or protoplanetary disks). In this case one should simply replace “black hole” with “central massive object” (e.g. star), and stellar disk with whatever collisionless disk surrounds the system. Because of the scale-free nature of the above equations, the rescaling of units is trivial.

3 THE WKB APPROXIMATION

First, consider modes in the limit of the WKB approximation of tight-winding (i.e. local modes), where $|kR| \gg m$. We caution that this limit does not, in fact, hold for most of the global modes seen in simulations, but it is nevertheless instructive.

3.1 Instability Criteria

The case of slow modes where the non-Keplerian part of the potential is everywhere small is presented in detail in Tremaine (2001). We briefly note some conclusions. Take the potential to be that of a central BH plus a non-Keplerian disk:

$$\Phi = \Phi_{\text{BH}} + \Phi_e = -\frac{GM_{\text{BH}}}{r} + \Phi_e \quad (17)$$

where $\Phi_e/\Phi_{\text{BH}} \sim M_d/M_{\text{BH}} \ll 1$. Further, consider “slow” modes, where the pattern speed $\Omega_p \ll \Omega$. We can expand the equations of motion in parameters of $\mathcal{O}(\epsilon)$ where $\epsilon \equiv M_d/M_{\text{BH}} \ll 1$. This gives the WKB dispersion relation (to leading order in $|kR|^{-1}$) of quasi-Keplerian slow modes,

$$\omega = \varpi + \pi G \Sigma_d |k| \Omega^{-1} - c_s^2 k^2 \Omega^{-1} \quad (18)$$

for a gas disk, or

$$\begin{aligned} \omega &= \varpi + \pi G \Sigma_d |k| \Omega^{-1} \mathcal{F} \\ &\approx \varpi + \pi G \Sigma_d |k| \Omega^{-1} \exp(-\beta |kR|) \end{aligned} \quad (19)$$

for a stellar disk, where we define

$$\begin{aligned} \varpi &\equiv \frac{\Omega^2 - \kappa^2}{2\Omega} \\ &= -\frac{1}{2\Omega} \left(\frac{2}{r} \frac{d}{dr} + \frac{d^2}{dr^2} \right) \Phi_d. \end{aligned} \quad (20)$$

In the dispersion relation for a stellar disk, \mathcal{F} is the standard reduction factor (Binney & Tremaine 1987), and the latter equality is a convenient approximation for softened gravity, with $\beta \approx \sigma_z/V_c \approx h/R$ (the stellar disk scale height).

It is obvious that all terms on the right-hand side of Equations 18-19 are real; therefore, quasi-Keplerian, “slow” $m = 1$ modes are stable at this order (for a more rigorous derivation, see Tremaine 2001).

We have, however, made a major assumption, that the disk mass is *everywhere* much less than the BH mass (and the mode is everywhere slow). In generality, and to second-order in $|kR|^{-1}$, the WKB dispersion relation can be written (for a gas disk)

$$(\omega - m\Omega)^2 = \kappa^2 + \left(k^2 + \frac{m^2}{r^2} \right) c_s^2 (1 + \chi) \quad (21)$$

$$- 2\pi G \Sigma_d \left(k^2 + \frac{m^2}{r^2} \right)^{1/2} (1 + \chi) \quad (22)$$

where

$$\chi = \frac{2}{1 + (kr/m)^2} \left(\frac{1-s}{1+s} \right); \quad s \equiv \frac{\partial \ln V_c}{\partial \ln R} \quad (23)$$

(Lau & Bertin 1978)¹

Whenever the right-hand side of Equation 22 is negative, the modes are unstable and grow exponentially. Take the case of interest, a global $m = 1$ mode in a relatively cold disk. For convenience take the limit $k = 0$ and $c_s = 0$; Equation 22 becomes

$$\left(\frac{\omega}{\Omega} - 1 \right)^2 = 2(1+s) - 2 \left(\frac{3-s}{1+s} \right) \tilde{f}_d \quad (24)$$

where

$$\tilde{f}_d \equiv \frac{\pi G \Sigma}{\Omega^2 R} \approx \frac{M_d(< R)}{M_{\text{enc}}(< R)} \quad (25)$$

is roughly the disk mass fraction inside R . The RHS is negative for $\tilde{f}_d > (1+s)^2(3-s)^{-1}$. If the potential is near-Keplerian, then $s \sim -1/2$, so this just becomes $\tilde{f}_d \gtrsim 1/10$.

In greater detail, consider the special case of a cold Mestel ($\eta = 1$) disk around a BH, with an $m = 1$ mode and mass ratio enclosed in some radius $y \equiv M_d(< R)/M_{\text{BH}}$; the full dispersion relation from Equation 22 is then

$$\left(\frac{\omega}{\Omega} - 1 \right)^2 = \frac{1}{1+y} \left[1 + 2y - y(|kR|^2 + 1)^{1/2} (1 + \chi) \right] \quad (26)$$

where for a local mode, $|kR| \gg 1$ and $\chi \rightarrow 0$, while for a global mode $|kR| \rightarrow 0$ but $1 + \chi \rightarrow (7 + 6y)/(1 + 2y)$. Global modes are formally unstable then for $y > (-3 + \sqrt{17})/4 \approx 0.281$ ($\tilde{f}_d = 0.11$), and local modes unstable for $|kR| > (1 + 2y)/y$. The solutions for arbitrary power-law disks η are tedious, but for global modes can be well approximated by $y > 0.07 + 0.09\eta + 0.07\eta^2 + 0.04\eta^3$.

More generally, for the power-law disk+BH and the stellar dispersion relation, the minimum radius at which instability appears (noting that the term $|kR| \exp\{-\beta|kR|\}$ is maximized for $|kR| = 1/\beta$) is given by

$$\frac{M_d(< R)}{M_{\text{BH}}} \geq \frac{\beta e}{(2 - \eta)(1 - \beta \alpha e(3 - \eta))}. \quad (27)$$

For small β this is just $y \gtrsim 1.35\beta(1 - \eta/2)^{-1}$. If the disk does not extend to these masses, then it will be everywhere locally stable. It is also immediately clear that if $\beta \geq 1/(\alpha e(3 - \eta))$ ($\approx 0.2 - 0.3$ for the interesting range of η), then the disk is everywhere locally stable independent of M_d/M_{BH} (this is just $Q \gtrsim 1$).

This instability criteria agrees well with what is seen in simulations; for the simulations discussed in § 1, the mode growth rate and maximum mode amplitudes are plotted as a function of M_d/M_{enc} at radii ~ 10 pc near the BH radius of influence in Figure 6 of Hopkins & Quataert (2010a) (see also Figure 12 of Hopkins & Quataert 2009). Around these values of y or \tilde{f}_d , rapid growth rates for the $m = 1$ mode appear at these radii. So at least at larger radii, mode growth is possible.

What is the nature of these modes? Note that the right-hand side of Equation 26 is real; as such, to lowest order in the WKB

approximation, the unstable branch must correspond to an *overstability* with the real part of ω , $\text{Re}(\omega) = \Omega_p = \Omega$. In other words, the system can develop *fast* modes that are globally unstable, where y is not very small.

This suggests a picture in which the $m = 1$ modes first appear at large radii – some R_{crit} where $M_d/M_{\text{BH}} \sim 1$, i.e. where the potential is only transitioning to Keplerian, and where it can be globally unstable. The pattern speed Ω_p will simply reflect $\Omega(R_{\text{crit}})$. But if the mode can propagate inwards at constant Ω_p , it will eventually be a slow mode, relative to the local Ω . This is, in fact, what is seen in simulations (see § 5 below).

3.2 Mode Structure and Propagation

How does this occur? For now, we will remain in the WKB approximation and consider how such a mode (stable or unstable) might evolve. Given a mode, the wave packets themselves propagate with approximate group velocity $v_g = d\omega/dk = \text{sign}(k)(c_s^2 - G\Sigma)/(\omega - \Omega)$ or $\pi G \Sigma \Omega^{-1} + 2c_s^2 k \Omega^{-1}$ for slow modes. For a cold disk this is simply $v_g \approx (\omega - \varpi)R|kR|^{-1}$; and since $\omega \sim \Omega(R_{\text{crit}})$ and the mode is global, this is $\sim V_c(R_{\text{crit}})$. The timescale for the mode to travel is just the dynamical time at this critical radius.

If the mass profile is too shallow, and c_s or σ remains constant at small radii, then the wave will refract back at some Q barrier at some minimum radius (for constant β , refraction occurs with $\eta < 1/2$, the same criteria that Ostriker et al. (1992) show applies for modes in a pure fluid disk with a hard outer edge). In non-linear simulations, this typically leads to pile-up of inflows, gradually steepening the profile; the consequences of this for setting galaxy profile shapes is discussed in Hopkins & Quataert (2010b). Here, the mass profile is fixed; but provided the mass profile is sufficiently steep such that the RHS of Equation 18 remains finite as $r \rightarrow 0$, then modes can propagate through to $R = 0$.

Provided that the sound speed is finite, wave packets in a gaseous disk can propagate through the OLR to $r \rightarrow \infty$, eventually becoming simple sound waves. This is discussed in Adams et al. (1989) – because the waves can freely escape carrying the mode energy and angular momentum (and will reflect off small radii as above), infinite pure gaseous disks in nearly-Keplerian potentials do not support strong growing modes. Instead, for gaseous disks, mode growth is sensitive to the description of the disk edge, and if a “hard” edge is assumed, specifically requires efficient reflection of waves off the outer edge. As a consequence, it is difficult to determine the growth rates for a pure gaseous disk without some *a priori* knowledge of the edge structure, and the derivations therein cannot be generalized in a straightforward manner to disks with smooth (or thick) edges. However, for a stellar disk, the mode cannot propagate beyond the OLR where $\Delta \equiv \kappa^2 - m(\Omega - \Omega_p)^2 = 0$ (this acts as an effective outer edge). Refraction of the stellar waves off this boundary is important, and means that mode growth is possible even when the disk extends to $R \gg R_{\text{OLR}}$. Together, these constraints set the dynamic range of the mode.

Physically, how can the mode propagate, if it “begins” at larger radii? It is easy to see as the eccentric mode at outer radii exciting strong eccentric perturbations at smaller radii. For a slow $m = 1$ mode near the BH (where the near-Keplerian approximation is good), the equations of motion for the perturbed velocity

¹ We follow (Lau & Bertin 1978) keeping in-phase terms to second-order in $|kR|^{-1}$ because the modes of interest are global ones. One can think of this as accounting for the effective minimum wavenumber m from the azimuthal wave, and including the enhancement $1 + \chi$ where $\chi = \Gamma \sin i$ ($\Gamma \equiv \partial \ln \Omega / \partial \ln R$ and i is the arm pitch angle), namely the leading-order term of the swing amplifier at this order in the WKB approximation.

$\mathbf{v} = R\Omega\hat{\phi} + v_r\hat{R} + v_\phi\hat{\phi}$ become, at this order,

$$v_r = -\frac{i}{2(\omega_p - \omega)} \left(\frac{d\Phi_e}{dr} + \frac{2\Phi_e}{r} \right) \quad (28)$$

$$v_\phi = \frac{i}{2} v_r \quad (29)$$

where Φ_e is the “external” perturbing potential from the larger-scale mode.

Consider an annulus R_1 , down to which the mode has efficiently propagated, and a slightly interior radius R_0 , which remains unperturbed. In the WKB limit the perturbing potential is dominated by the local structure – so just interior to R_1 it is $\approx \Phi_1(R_1) = 2\pi G \Sigma_1(R_1) |k|^{-1}$. There is no local corrugation present at R_0 or interior (by definition) to cancel this perturbation term. This applies as well in the global (non-WKB) limit; consider the limiting case of an element on a circular orbit inside an eccentric ring with mass M_{ring} at radius R_1 (with $m = 1$ mode amplitude $|a|$ defining the eccentricity of the ring). The magnitude of the asymmetric term in the potential just inside R_1 is $\approx |a| G M_{\text{ring}} / R_1 \sim \pi G \Sigma_1(R_1) R_1$. If the disk is cold, then the local pattern speed is given directly by $\omega - \varpi \approx \pi G \Sigma_0 |k| \Omega^{-1}$. Taking these estimates for the potential perturbation and pattern speed and applying them in Equation 28, we obtain

$$v_r = -\frac{\Sigma_1}{\Sigma_0} |kR|^{-1} \Omega R \quad (30)$$

$$|e| \sim \left| \frac{v_r}{V_c} \right| = \frac{\Sigma_1}{\Sigma_0} |kR|^{-1} = \frac{|a|}{|kR|} \sim |a|. \quad (31)$$

For non-trivial mode amplitude $|a| \sim \Sigma_1/\Sigma_0$, and a global mode $|kR| \sim 1$, corresponding eccentricities and coherent $m = 1$ mode amplitudes are induced. This of course can then induce eccentricity at the next smaller annulus, and so on, allowing the perturbation to grow even at small R . By the same arguments, at much steeper slopes $\eta \gtrsim 1$, the system will become more “stiff” against inwards propagation of eccentricity, but there is no strict cutoff/refraction (see also Zakamska & Tremaine 2004, who find the same for disks of planets and planetesimals).

The key facet to note is that for an “external” driver of the perturbation Φ_e , the response is large independent of the local ratio of disk to BH mass, and is linear in Φ_e . Thus, the mode only needs to be locally unstable *somewhere* in order to self-amplify (recall, our stability analysis is in the WKB limit and hence local). Self-gravity will grow the strength of the mode there, but the system will respond coherently at small radii, even where the system is nominally stable (a local mode there would not self-amplify).

Finally, in both gas and stars, near the inner refraction radius (for $\eta \lesssim 1/2$), an initially global mode must wind up to $|k| \sim \Omega c_s^{-1}$ or $|k| \sim \Omega \sigma_z^{-1}$, respectively. Near the OLR or $r \rightarrow 0$ (if $\eta \gtrsim 1/2$) in stars, then $|kR| \exp\{-\beta|kR|\} \rightarrow 0$ so there are the standard two branches: long $|kR| < \beta$ and short $|kR| > \beta$. The long branch solution corresponds to the extension of the g -modes described in Tremaine (2001), but for $\eta \gtrsim 1/2$ and an OLR out at large radii where M_d/M_{BH} is not small, they do not have to have negative (retrograde) pattern speeds. The short branch corresponds to the p -modes described there.

4 EXACT SOLUTIONS

The WKB approximation has been instructive. However, this does not allow us to survey the complete parameter space, and it is a suspect approximation for any global mode with small $|kR|$. Therefore, it is important to check our conclusions and examine the mode

structure in exact solutions to the perturbed linear equations of motion.

4.1 Equations of Motion

We must choose a specific disk model, so for convenience, adopt the power-law model in § 2. We can freely define R_0 anywhere; so choose it such that (for the infinite disk) $M_d(< R_0) = [\alpha(2 - \eta)]^{-1} M_{\text{BH}}$ – i.e. $\Sigma_0 = M_{\text{BH}}/(2\pi\alpha R_0^2)$. We can then still apply any disk cutoff with a in units of R_0 determining the ratio M_d/M_{BH} . We will consider all numerical quantities in units $M_{\text{BH}} = G = R_0 = 1$.

Following Tremaine (2001), define the perturbed quantities as $\Sigma(r) + \Sigma_1(\mathbf{r}, t)$, $\mathbf{v}_d(r) + \mathbf{v}_1(\mathbf{r}, t) = r\Omega\hat{\phi} + u_1(\mathbf{r}, t)\hat{r} + v_1(\mathbf{r}, t)\hat{\phi}$, $\Phi(r) + \Phi_1(\mathbf{r}, t)$, and in standard fashion write the perturbation variables in the form $X_1(\mathbf{r}, t) = X_1(r, \phi, t) = X_a(r) \exp[i(\phi - \omega t)]$. The equations of motion, together with Poisson’s equation, can be written

$$i(\Omega - \omega)\Sigma_a = -\frac{1}{r} \frac{d}{dr} (r \Sigma u_a) - \frac{i}{r} \Sigma v_a \quad (32)$$

$$u_a = -\frac{i}{\Delta} \left[(\Omega - \omega) \frac{d}{dr} + \frac{2\Omega}{r} \right] \Phi_a \quad (33)$$

$$v_a = \frac{1}{\Delta} \left[\frac{\kappa^2}{2\Omega} \frac{d}{dr} + \frac{(\Omega - \omega)}{r} \right] \Phi_a \quad (34)$$

$$\Delta = \kappa^2 - (\Omega - \omega)^2 \quad (35)$$

$$\Phi_a = \int_0^\infty dr' r' P(r, r') \Sigma_a(r') \quad (36)$$

$$P(r, r') = P_{\text{direct}}(r, r') + P_{\text{indirect}}(r, r') \quad (37)$$

$$= -\frac{\pi G}{r_{>}} b_{1/2}(r_{<}/r_{>}) + \frac{\pi G r}{r'^2}$$

where the kernel P for the potential includes the direct (what would appear even in an inertial frame) and indirect components. The Laplace coefficient $b_{1/2}$ is given by

$$b_{1/2}(x) = \frac{2}{\pi} \int_0^\pi \frac{\cos \theta d\theta}{(1 - 2x \cos \theta + x^2 + \beta^2)^{1/2}} \quad (38)$$

where β represents the gravitational softening.² We choose this particular softening both because it is numerically convenient, and because it reduces exactly to the solution for a disk with scale height $\beta = h/R$ (with $\rho = \Sigma/2h$ at $|z| < h$) when $h \ll R$.

This formulation of the indirect potential follows Murray & Dermott (2000). The inclusion of the indirect potential is necessary because the $m = 1$ mode changes the center of mass, leading to motion by the BH about that center of mass. Recall that our coordinate frame is centered on the BH, thus r is the vector distance to the BH, and the frame is rotating about the BH.

For a given ω , η , and β , then, the solution to these coupled equations determines the perturbation structure. Because we are interested in the behavior where ω/Ω may be non-trivial, the equations are non-linear in ω . However, we can combine the equation in

² Note that when we soften the gravity for the perturbation, we also soften that of the unperturbed disk. This leads to a slight change in the disk potential, and hence Ω and κ given in § 2 for a cold disk. However, the difference is very small (usually $< 2\%$), and has no effect on our conclusions (compared to simply using $\Omega(R)$ of a cold disk).

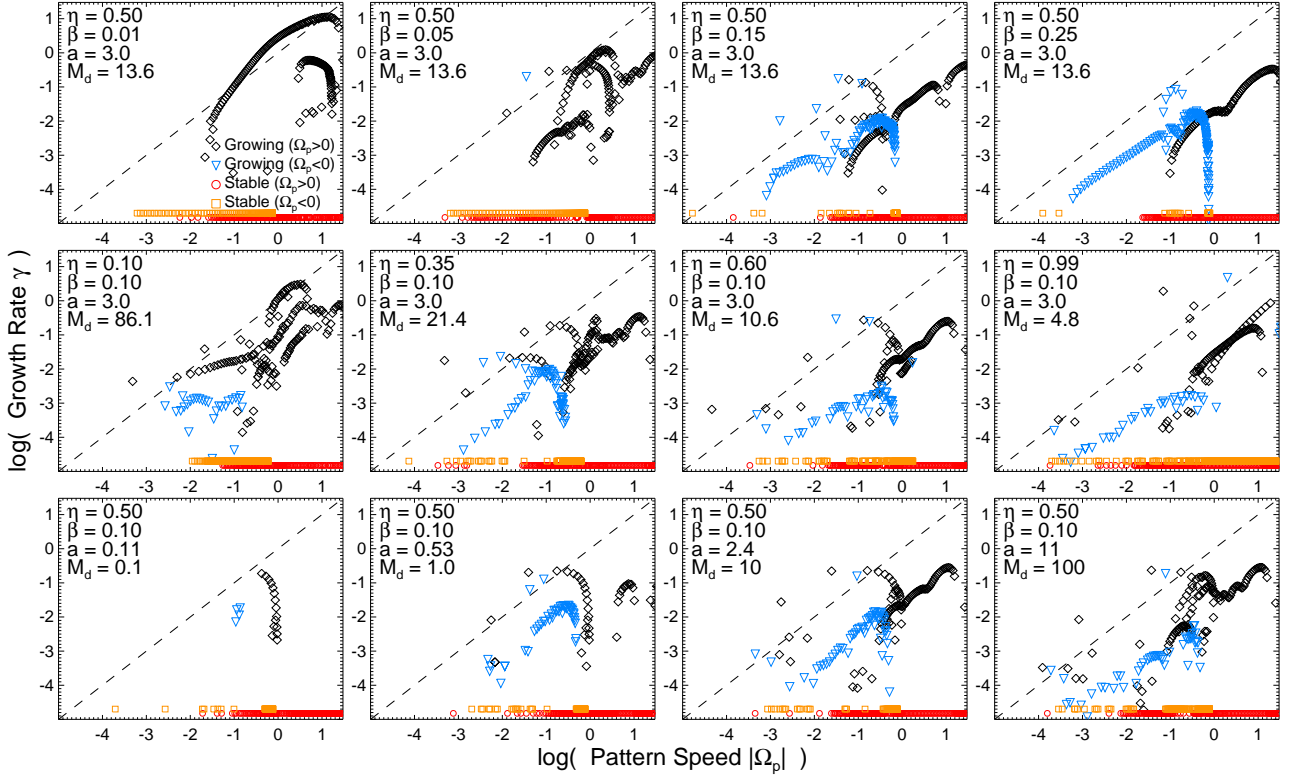


Figure 1. Spectrum of eigenvalues (normal mode frequencies) for $m = 1$ modes in the truncated power-law disk in Equation 14 around a BH, in units of $M_{\text{BH}} = R_0 = G = 1$, as a function of the parameters β (the disk softening $\sim h/R$), η (the mass profile slope) and a (the outer disk scale length, which determines the disk-to-BH mass ratio M_d/M_{BH}). Black diamonds show the pattern speed Ω_p and growth rate γ for growing modes ($\gamma > 0$). Stable modes ($\gamma = 0$) are shown for comparison (red circles at $\gamma = 10^{-5}$ just to be displayed). Blue triangles show growing modes with $\Omega_p < 0$ (retrograde precession), plotting $|\Omega_p|$. For comparison, the dashed line corresponds to $\gamma = |\Omega_p|$. There is a large spectrum of (mostly prograde) rapidly-growing modes with $\gamma \sim \Omega_p$, and growth rates that increase in colder and relatively more massive disks. Non-zero growth rates can be present even in disks that are locally stable ($Q \gg 1$) and disks with small $M_d/M_{\text{BH}} \sim 0.1$.

Σ_a , u_a , and v_a to obtain a single equation

$$\begin{aligned}
 0 = & -(\Omega - \omega) \Sigma_a \\
 & + \frac{\Sigma}{r^2 \Delta} [2\Omega(\nu_\Sigma + \nu_\Omega - \nu_\Delta) - (\Omega - \omega)] \Phi_a \\
 & + \frac{\Sigma}{r \Delta} \left[(\Omega - \omega)(1 + \nu_\Sigma - \nu_\Delta) + \Omega(2 + \nu_\Omega) - \frac{\kappa^2}{2\Omega} \right] \Phi'_a \\
 & + \frac{\Sigma}{\Delta} [\Omega - \omega] \Phi''_a
 \end{aligned} \quad (39)$$

Where $\Phi' = \int dr' r' (\partial P(r, r') / \partial r) \Sigma_a(r')$ and $\Phi'' = \int dr' r' (\partial^2 P(r, r') / \partial r^2) \Sigma_a(r')$, and $\nu_X \equiv \partial \ln X / \partial \ln r$. If we discretize Σ_a into some grid in $\log r$ and apply some summation rule to evaluate the integrals in Φ , then we can write this as a linear operator acting on the perturbed density,

$$\mathbf{M} \bar{\Sigma}_a(\vec{r}) = \vec{0} \quad (40)$$

The eigenvalues ω and eigenvectors $\bar{\Sigma}_a$ represent the exact homogenous solutions to this equation. In practice, we obtain solutions following the method outlined in Appendix B of Adams et al. (1989). If we multiply Equation 39 by Δ^2 , then we can eliminate all occurrences of ω in the denominator and write the resulting matrix equation as a fifth-order equation in ω : $(\mathbf{M}_0 + \omega \mathbf{M}_1 + \omega^2 \mathbf{M}_2 + \omega^3 \mathbf{M}_3 + \omega^4 \mathbf{M}_4 + \omega^5 \mathbf{M}_5) \bar{\Sigma}_a(\vec{r}) = 0$ where the \mathbf{M}_n are independent of ω . With the appropriate substitutions, this can then be turned into a single eigenvalue equation $\mathbf{M}_{5 \times 5} \bar{T}_a = \omega \bar{T}_a$, where if \mathbf{M} is $N \times N$ elements, $\mathbf{M}_{5 \times 5}$ is $5N \times 5N$, and $\bar{T}_a =$

$(\bar{\Sigma}_a, \mathcal{O}(\omega \mathbf{M}_1)^1 \bar{\Sigma}_a, \mathcal{O}(\omega \mathbf{M}_1)^2 \bar{\Sigma}_a, \mathcal{O}(\omega \mathbf{M}_1)^3 \bar{\Sigma}_a, \mathcal{O}(\omega \mathbf{M}_1)^4 \bar{\Sigma}_a)$ is constructed from combinations of the \mathbf{M}_n , $\bar{\Sigma}_a$ and ω . It is then straightforward to solve for all eigenvalues and eigenvectors.³

4.2 Results

4.2.1 Growth Rates

Figure 1 illustrates the spectrum of eigenvalues of growing modes, in power-law disks, as a function of the softening (β), slope (η), and disk cutoff radius/mass (a). For now, we simply show all eigenvalues of the above equations that fall in the plotted range, making no discrimination between local or global modes. We focus on the growing modes, but see that in all cases there is a very large spectrum of stable modes; there are also decaying modes, but these correspond to the complex conjugate pairs of the growing modes shown.

The nearly continuous lines traced out by the eigenvalues correspond to solutions that cover some finite dynamic range well in-

³ Numerically, we typically realize this on a grid of $\sim 400 - 4000$ elements evenly spaced in $\log r$ from a factor of several outside of the OLR, where the mode amplitude vanishes, to $r \sim 10^{-5} R_0$. The results are numerically converged. Normalizing such that $|\bar{\Sigma}_a| = N$, where N is the number of grid points, and $|\text{Row}(\mathbf{M})| = N$ for each row of \mathbf{M} , we obtain solutions of $\mathbf{M} \bar{\Sigma}_a(\vec{r}) = \vec{\delta}$ with typical $|\vec{\delta}|/N \lesssim 10^{-16}$.

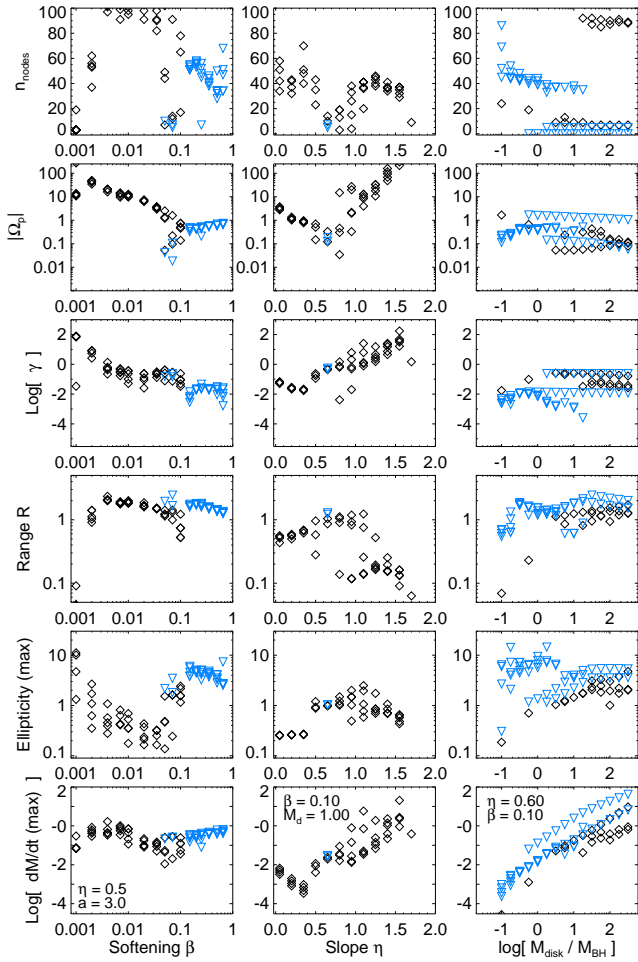


Figure 2. Scaling of the largest dynamic-range growing ($\gamma > 0$) normal modes (largest five $\mathcal{R} \equiv \int |a| d \log R$). *Left:* At fixed slope and a , M_d , as a function of β . *Center:* As a function of slope η (varying a to hold $M_d = M_{\text{BH}}$). *Right:* As a function of M_d (and a). In each column, we show the number of zero-crossings n , the mode pattern speed $|\Omega_p|$ (black have $\Omega_p > 0$, blue have $\Omega_p < 0$), the growth rate γ , the range \mathcal{R} , the maximum ellipticity $\equiv R_1/R$ induced by the mode (mode amplitude normalized so that $\text{MAX}(|a|) = 1$), and the maximum inflow rate induced (units of $M_0 (GM_0/R_0^3)^{-3/2}$; for a BH this is $8400 f_{\text{gas}} M_\odot \text{yr}^{-1} (M_{\text{BH}}/10^8 M_\odot)^{3/2} (R_0/4 \text{pc})^{-3/2}$; for a protostellar/circumstellar disk $0.2 f_{\text{gas}} M_\odot \text{yr}^{-1} (M_*/M_\odot)^{3/2} (R_0/10 \text{au})^{-3/2}$).

side the cutoff a (i.e. where the disk is still scale-free), so that the solution can simply be shifted in r and ω . Broadly speaking, the growing modes range in growth rates from $\gamma \sim 0.01 - 1 |\Omega_p|$, and the pattern speeds Ω_p for both stable and growing modes tend to fall in a similar range. We will show how this relates to the characteristic scales of the modes below.

At fixed η and a (or M_d/M_{BH}), increasing the softening β decreases the mode growth rates $\gamma/|\Omega_p|$, and decreases the overall fraction of unstable modes, as expected. However, growing modes exist even for large $\beta \gtrsim 0.25$. These are global modes, where there is a large contribution to the instability from the indirect potential, which is not treated in the WKB limit. Hence, our previous conclusions regarding sufficient β for stability should be regarded as only pertaining to local instabilities. Adams et al. (1989) found similar results, in that global instability could appear even in $Q \gg 1$ (everywhere locally stable) disks.

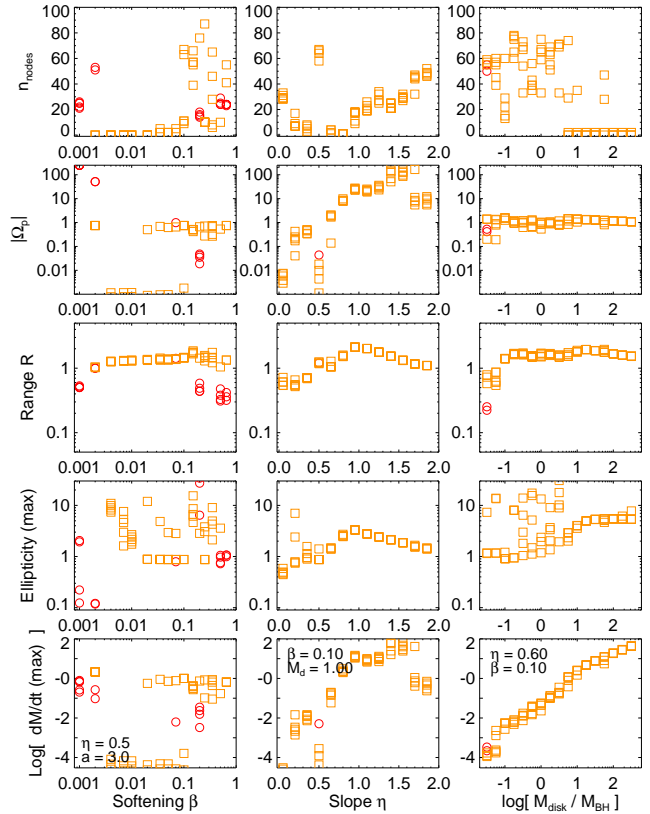


Figure 3. As Figure 2, but for the largest dynamic range stable ($\gamma = 0$) modes. The scalings are similar – the major difference is the existence of stable (but not unstable) modes at $M_d \ll M_{\text{BH}}$.

Modes with moderate or large negative (retrograde) pattern speeds, $\Omega_p \ll -1$ are generally not supported. Some modes with small retrograde pattern speeds are supported, increasingly at large β and/or η . However, such modes will tend to drive outflows (though not in every case), so in practice may not be able to self-consistently build up a disk to the steep surface density profiles ($\eta > 1/2$) needed to support them in the first place.

At fixed β and a/R_0 , modes with lower η (shallower disk profiles) have somewhat larger growth rates, but the effect is most pronounced only as $\eta \rightarrow 0$. This is partly an artifact of holding a/R_0 fixed, since doing so while decreasing η means that M_d/M_{BH} is larger in the lower- η disks. But there is also a (small) real effect because relatively less of the disk mass is at very small radii where the BH dominates the potential. The range of unstable modes is similar, though, and we see below that these modes propagate over a smaller dynamic range in radius.

At fixed η and β , changing a and correspondingly M_d has the expected effect – at larger M_d/M_{BH} , growth rates (and the fraction of unstable modes) increases. Also, the maximum speed of the unstable modes increases, as we might expect from the WKB analysis (since the supported mode speeds scale with M_d/M_{BH} in the nearly-Keplerian limit). There are still significant unstable modes even at low a and M_d though – they appear at approximately $M_d \sim 0.1$. So although it is true that in the limit of vanishingly small M_d/M_{BH} , all modes are stable, in practice given the right mass profile and softening, a small finite M_d/M_{BH} can still give interesting mode growth.

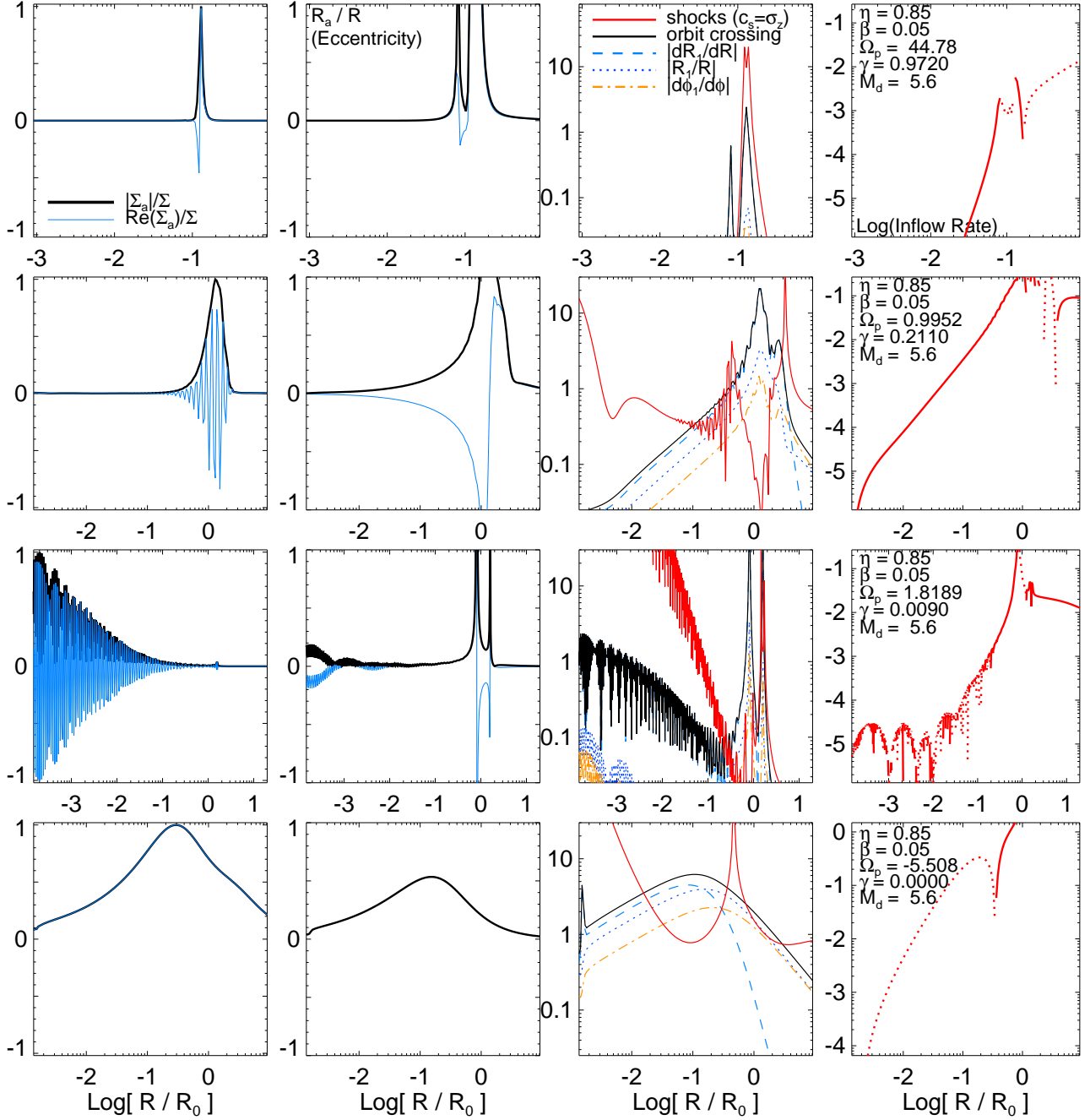


Figure 4. Example eigenmodes of the $m=1$ mode in a BH+power-law disk with softened gravity. Each row shows the properties of one such mode, with parameters at right (disk mass profile slope $\Sigma \propto R^{-\eta}$, softening $\beta \sim h/R$, pattern speed $\Omega_p = \text{Re}(\omega)$, mode growth rate $\gamma = \text{Im}(\omega)$, and disk-to-BH mass ratio M_{disk}). Radii are in units of R_0 (the radius where the enclosed disk mass $\sim M_{\text{BH}}$). Modes are shown from an outer radius outside the OLR (where they terminate) to $\sim 10^{-3} R_{\text{OLR}}$. *Left:* Mode amplitude. The absolute magnitude of the density perturbation $|\Sigma_a|/\Sigma$, and $\text{Re}(\Sigma_a)/\Sigma$ (the latter shows the wavenumber, i.e. $\exp[i \int k dr]$). *Center-Left:* Induced radial perturbation $\equiv R_a/R$ (equal to the eccentricity, in the near-Keplerian regime). *Center-Right:* Conditions for orbit-crossing. The perturbation radii $|R_1|/R$, $\zeta = |dR_1/dR|$, and $|d\phi_1/d\phi|$. The “all” line is $(|R_1|/R)^2 + |dR_1/dR|^2 + |d\phi_1/d\phi|^2$. If any are > 1 , there are orbit crossings. Red line shows the criterion from Equation 44, for where gas shocks will be induced (when > 1); note this can occur even without formal orbit crossings. *Right:* Log of the gas inflow (solid) or outflow (dotted) rate $|\dot{M}|$ driven by the mode, in units of $f_{\text{gas}} M_{\text{BH}} \Omega_0$, where $\Omega_0 \equiv (GM_{\text{BH}} R_0^{-3})^{1/2}$. In the units here, 1 corresponds to $8400 M_{\odot} \text{yr}^{-1} (M_{\text{BH}}/10^8 M_{\odot})^{3/2} (R_0/4 \text{pc})^{-3/2}$ for a BH, or $0.20 M_{\odot} \text{yr}^{-1} (M_*/M_{\odot})^{3/2} (R_0/10 \text{au})^{-3/2}$ for a circumstellar disk. The (arbitrary) mode amplitudes are normalized so $\text{MAX}(|\Sigma_a|/\Sigma) = 1$. The figure shows several modes with different Ω_p and γ in a fixed system. The largest γ and Ω_p mode (top) is local; at lower Ω_p (middle) the modes cover a larger dynamic range, but still have moderate $|kR|$; the most global mode (bottom) is stable, and retrograde.

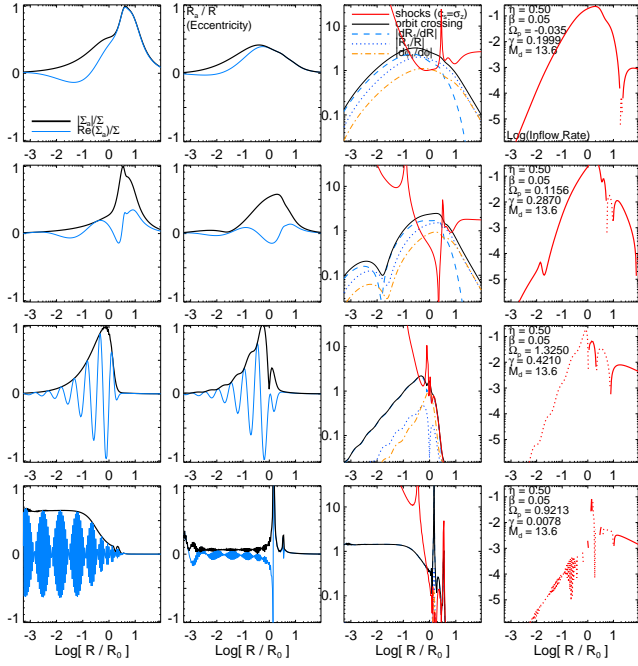


Figure 5. Figure 4 continued. Mode structure versus n , the number of nodes, in the growing modes of an otherwise fixed system. From top to bottom, n increases from 2 to > 100 . The moderate- n modes have similar Ω_p and larger γ . Despite large n , some of these modes are clearly very long-wavelength.

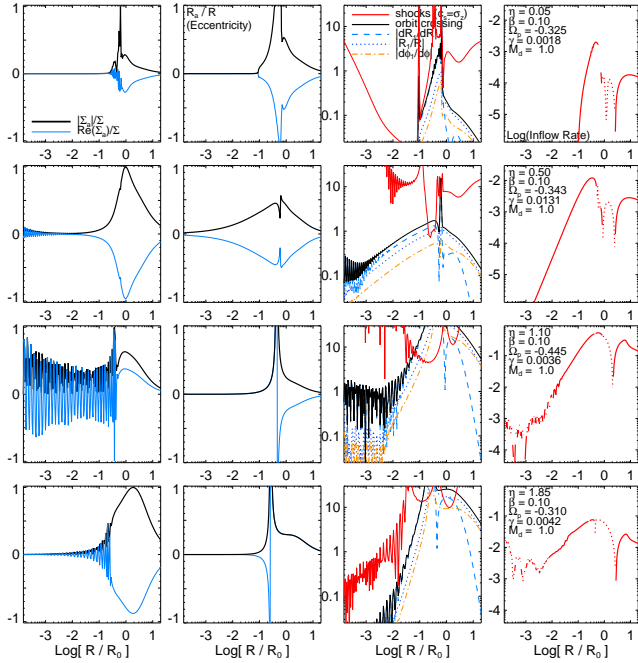


Figure 6. Figure 4 continued. Mode structure versus mass profile slope η at otherwise fixed properties (top-to-bottom: $\eta = 0.05, 0.5, 1.1, 1.85$). For shallow slopes $\eta < 1/2$, the mode at fixed β cannot be supported at $R \rightarrow 0$, and so it is localized. At larger η , the modes carry amplitude at $R \rightarrow 0$.

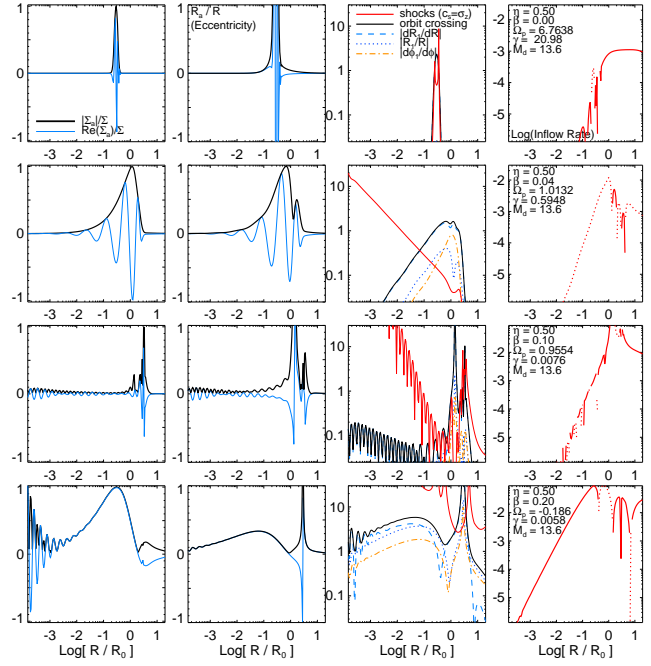


Figure 7. Figure 4 continued. Mode structure versus gravitational softening/disk scale height at otherwise fixed properties (top-to-bottom: $\beta = 0.002, 0.04, 0.1, 0.2$). Modes with otherwise similar properties are more global in softened/thick disks, and more tightly-wound in cold disks. A sufficiently cold disk does not support the same global modes because the implied growth rate at large radii is much larger than that at small radii.

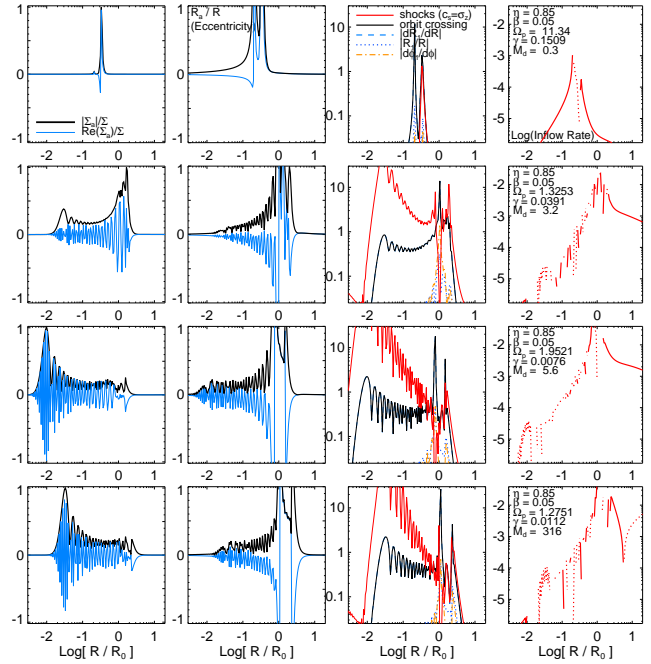


Figure 8. Figure 4 continued. Mode structure versus disk-to-BH mass ratio at otherwise fixed properties (top-to-bottom: $M_{\text{disk}}/M_{\text{BH}} = 0.31, 3.2, 5.6, 316.3$). At low M_{disk} , the most unstable (local, high- k) modes appear first. Higher $M_{\text{disk}} \sim M_{\text{BH}}$ allows more global modes. Once $M_{\text{disk}} \gtrsim M_{\text{BH}}$, the structure of modes that exist at small radii (the nearly-Keplerian regime) is similar regardless of M_{disk} .

4.2.2 General Mode Properties

To see how the mode properties scale in detail with these choices, we need to select some subset of modes to study. Typically, modes are compared at fixed n_{nodes} , the number of nodes or zero-crossings. However, because of the large scale-free range, there are many modes with the same n ; moreover, with the large dynamic range involved, the $n = 0$ modes are not necessarily the “most global” (they might cover only a limited range in radius). Since we are interested in modes that cover a large dynamic range, we define the proxy

$$\mathcal{R} \equiv \int_0^\infty |a(R)| d \log R \quad (41)$$

where the (arbitrary) normalization of the mode amplitude is set such that $\text{MAX}(|a(R)|) = 1$ (the maximum value for which the solution would not imply negative densities somewhere). Roughly speaking, a couple times \mathcal{R} gives the number of dex over which the mode has a significant amplitude.

In Figure 2, we select the five growing ($\gamma > 0$) modes with the largest values of \mathcal{R} , and show how their properties scale with β , η (in this case, allowing a to vary to hold M_d/M_{BH} fixed while η varies), and the disk mass M_d . In Figure 3, we show the same, but for the largest- \mathcal{R} stable ($\gamma = 0$) modes. We show a number of mode properties: the number of nodes n_{nodes} , the pattern speed $|\Omega_p|$, growth rate γ (for the unstable modes), and range \mathcal{R} defined above. We are also interested in the effect of the perturbation on eccentricities and, ultimately, inflow. The magnitude of the radial perturbation $|R_1|/R$ from a given mode is, for linear perturbations,

$$R_1 = -\frac{1}{\Delta} \left(\frac{d\Phi_1}{dR} + \frac{2m\Omega}{R(m\Omega - \omega)} \Phi_1 \right) \quad (42)$$

Defining the eccentricity as $|e| = (r_a - r_p)/(r_a + r_p) = |R_1|/R$, we plot the maximum $|e|$ induced by the mode over all radii, given the same normalization condition $\text{MAX}(|a(R)|) = 1$. If the eccentricities are anywhere significant, there can be orbit crossings, hence shocks and dissipation. So we can calculate the induced gas inflow rates, using the scalings derived in Hopkins & Quataert (2010a), for the inflow rates of gas driven by shocks induced by gravitational instabilities. They show

$$\dot{M} = \Sigma_{\text{gas}} R^2 \Omega \left| \frac{\Phi_1}{V_c^2} \right| \frac{m \text{sign}(\Omega - \Omega_p)}{1 + \partial \ln V_c / \partial \ln R} F(\zeta, \Phi_1) \quad (43)$$

where $F(\zeta, \Phi_1) = f(\zeta) S(\zeta, \Phi_1, \omega)$ includes a weak, non-linear function of the induced motions from the perturbation ($f(\zeta)$ where $\zeta \equiv \partial R_1 / \partial R$; with $1/2 < f(\zeta) < 2$ for all ζ) and the phase function S that depends on the relative phases of the overdensity/potential amplitude and radial motions/shock locations ($-1 < S < 1$), which determines whether the gas is inflowing ($\dot{M} < 0$) or outflowing ($\dot{M} > 0$). We show the resulting maximum $|\dot{M}|$, given the same normalization condition.

We see many of the same trends as in Figure 1, in greater detail. With increasing β , the growth rates (and pattern speeds, $|\Omega_p| \sim |\gamma|$) decrease, but the dynamic range covered by the modes increases weakly. The latter simply comes from the fact that the softening suppresses local modes and increases the dynamic range over which the disk is in effective contact. The decrease in γ with β is especially striking if one considers the fastest-growing modes (mostly local, therefore not plotted here). The maximum inflow rates scale weakly, decreasing at high- β as expected due to the increased stiffness. At high β we see the increased prominence of retrograde modes as in Figure 1, and in fact these dominate the high- \mathcal{R} modes. Recall, at small radii the WKB dispersion relation

reduces to Equation 19, which maximizes ω at $|kR| = 1/\beta$, giving for the power-law disk $\omega_{\text{max}} = (e^{-1} \beta^{-1} - \alpha(2 - \eta)) \pi G \Sigma / \Omega R$. Thus, when $\beta > 1/(e \alpha(2 - \eta))$, $\omega_{\text{max}} < 0$, and only retrograde modes are supported at small radii. As a consequence, prograde modes, although they exist, will tend to cover a relatively smaller dynamic range.

We see even at fixed M_d , the trend that γ increases with increasing slope η . The pattern speed Ω_p increases with γ . The inflow rates increase towards steeper η , which simply comes from the fact that there is proportionally more disk mass at small R . There is also significant change in dynamic range. From $\eta \approx 0 - 0.5$, \mathcal{R} increases by a factor of 2–3 with η , to a peak at $\eta \approx 1$, and then declines. This comes from the behavior discussed in § 3.2, wherein modes at $\eta < 1/2$ cannot propagate efficiently to $R \rightarrow 0$, while modes at $\eta > 1$ can technically propagate but do so with declining efficiency (see Hopkins & Quataert 2010b). The effect is large: mode dynamic range goes from ~ 0.1 dex to ~ 2 dex in the unstable modes or 0.5 dex to 5 dex in the stable modes.

Changing the disk mass M_d/M_{BH} , we also obtain a number of interesting trends. For the chosen η and β , unstable modes first appear at $M_d/M_{\text{BH}} \sim 0.1$; the criterion depends somewhat on these quantities, but in general we find it agrees more or less with our WKB instability criterion in Equation 27. At smaller M_d/M_{BH} , there are only stable modes – these persist at arbitrarily small M_d/M_{BH} and can still drive quite significant eccentricities and inflow rates, and at sufficiently small M_d/M_{BH} their properties can be well-approximated by the derivations in Tremaine (2001). Once instability arises, there is only a weak dependence of the growth rate and Ω_p on M_d/M_{BH} , however (it is largely determined by Ω at the radius where M_d reaches this threshold mass). Inflow rates increase approximately in proportion to the disk mass.

4.2.3 Mode Structure

Figures 4–8 illustrate some of the eigenvectors (normal modes) for a range of eigenvalues ω , for representative choices of η and β . We focus on the global modes; there are of course a wide spectrum of local modes available on large scales of the self-gravitating disk. In each Figure, we plot the mode amplitude $|a(R)|$, as well as $\text{Re}(\Sigma_a/\Sigma) = |a(R)| \exp\{i \int^r k dr\}$, which shows the winding and corrugations of the modes. The surface density perturbations generically experience sharp gradients and reflect off the OLR ($\text{Re}(\omega) = \Omega + \kappa$, $r \sim a$ few), although in some cases the $\Sigma_a \rightarrow 0$ earlier, at COR (a typical factor ~ 3 smaller radius).

We also plot the vector radial perturbation, defined for simplicity here as just R_a/R ($|R_a/R|$ is equivalent to the standard scalar eccentricity in the nearly-Keplerian regime; also in this regime $|R_a/R| \approx |v_a/V_c|$ where the velocity perturbation $v_{1,R} = dR_1/dt$). This clearly reflects the Σ perturbation.

We also show the magnitude of the radial perturbation, $|R_1|/R$ (defined above) along with the magnitude of its dimensionless derivative, $|dR_1/dR|$, and the same for the azimuthal perturbation ϕ_1 . If these quantities exceed unity, there are orbit crossings, therefore shocks and gas dissipation. Note that orbit crossings can occur, in principle, even if these quantities do not exceed unity – this is only an approximate guideline. In fact, Hopkins & Quataert (2010a) show that in a disk with finite gas sound speed c_s , there can be gas collisions and shocks, even where there are no orbit crossings. The requirement for dissipative encounters is that gas streams moving in the potential of the mode be compressed by the torques from the collisionless component at a velocity greater than c_s . This

condition can be written

$$\xi \equiv \frac{2\pi Q}{1 - |dR_1/dR|} \frac{1}{\kappa} \left(\left| \frac{\partial v_{1,R}}{\partial R} \right|^2 + \left| \frac{\partial v_{1,\phi}}{\partial R} \right|^2 \right)^{1/2} \geq 1 \quad (44)$$

where $Q = c_s \kappa / \pi G \Sigma$. This depends on the gas sound speed c_s , so is not determined in the collisionless models here, but if we assume the gas in these disks has $c_s \sim \sigma_z$, then we can determine ξ . The results are plotted; at small radii especially, $\xi \gg 1$ is common – for disks with finite $c_s \sim \sigma_z$ in their gas, shocks will be common (owing to the large $\sim V_c$ radial motions of the eccentric modes) at small radii, even when formal orbit crossings are rare.

Finally we show the induced inflow/outflow rates, using the scaling in Equation 43 to determine the gas inflow response to the stellar+BH potential. Because of our choice of units, these inflow rates are in units of $f_{\text{gas}} M_{\text{BH}} (GM_{\text{BH}}/R_0^3)^{1/2}$, where $f_{\text{gas}} = M_{\text{gas}}/M_*$ is the gas mass fraction in the disk. The inflow rates can be quite large for the systems of interest – given typical numbers, a rate of $\sim 10^{-4}$ in these plots corresponds to $\sim 0.1 - 1 M_\odot \text{yr}^{-1}$ accretion rates onto a supermassive BH, or $\sim 10^{-5} M_\odot \text{yr}^{-1}$ onto a star.

Now, consider specifically Figures 4-5, which illustrate modes with different frequencies and radial wavenumbers, for a fixed disk system. We see several of the behaviors discussed in § 5: the modes are global in dynamic range, but can have sizeable $|kR|$ and a large number of nodes. Since the slopes here are steeper than or equal to $\eta = 1/2$, the modes can exist down to $r \rightarrow 0$. Modes with smaller pattern speed extend to larger radii (the OLR moves out) and can sustain their amplitude over a larger dynamic range, while modes with $\text{Re}(\omega) \gg 1$ are not supported at moderate to large radii. Modes with large negative pattern speed are not seen; but those with moderate pattern speed are present and are among the most long-wavelength modes. This behavior is similar to that of the g -modes in Tremaine (2001) – however, that work concluded that when the disk mass is negligible compared to the BH mass, such modes cannot be supported in an isolated BH+disk system; here, we find that moderate disk-to-BH mass ratios allow for their existence.

The induced velocity perturbation and eccentricities are large, and reflect the mode density structure. Where present, orbit crossings tend to occur between the COR and OLR ($R \sim R_0$), and at the smallest radii. However, one is rarely in the strong orbit-crossing regime – there seems to almost be a maximum $|dR_1/dR| \sim 1$. This is easy to understand from the WKB analysis: recall, we showed that in the nearly-Keplerian, low disk mass limit, $|v_r/V_c| \approx |a|/|kR|$. Since we are nearly Keplerian, it is trivial to show that correspondingly $|R_1/R| \approx |v_r/V_c|$. And in the WKB limit, $d/dR = ik$, so $|dR_1/dR| \approx |a|$. Since $|a| < 1$ always, we do not expect to see dramatic orbit crossings. However, the criteria for shocks, from Hopkins & Quataert (2010a), is satisfied over a wide range of radii with $\xi \gg 1$. This occurs because the perturbation velocities are a fixed fraction $\sim |a|/|kR|$ of V_c , and so diverge at small radii – thus even without formal orbit crossings, gas is being compressed in the mode at velocities $\gg c_s$ at small radii, generating shocks and dissipation.

This, correspondingly, allows for the inflow rates calculated (wherever $\xi \gtrsim 1$). The inflow rates drop towards $R \rightarrow 0$, as seen in hydrodynamic simulations (see Figures 5 & 12 in Hopkins & Quataert 2009). But given the choice of units here, they are still quite large at radii $\sim 10^{-3} - 10^{-2} R_0$, where for the appropriate choice of Ω_p and η , they often asymptote to approximately constant $\dot{M}(R)$. Recall again the units used: if the value in Figure 4 is \tilde{m} , then the implied Eddington ratio of the BH is $\dot{M}/\dot{M}_{\text{Edd}} \approx 892 \tilde{m} f_{\text{gas}} (M_{\text{BH}}/10^8 M_\odot)^{1/2} (R_0/10 \text{ pc})^{-3/2}$, or $508 \tilde{m} f_{\text{gas}} (M_{\text{BH}}/10^8 M_\odot)^{-1/4} (\Sigma_0/10^5 M_\odot \text{pc}^{-2})^{3/4}$. So the im-

plied accretion rates at these radii are about Eddington, for a mode of near-maximal strength. This is important, since these are the radii where we expect the viscous disk to take over – inside such a radius, the ratio of the disk to BH mass is as low as $\sim 10^{-5}$, so Q becomes extremely large and we expect star formation (and thus the role of the collisionless component) to be inefficient. For a circum-stellar disk, these radii approach the stellar radius itself.

In Figure 6, we consider how the modes depend on the disk mass profile slope η . When the slope is shallow, the modes are confined to larger radii; at $\eta \sim 0.5 - 1.0$ mode amplitudes propagate to $R \rightarrow 0$; and at much larger η the relative amplitude can be damped at smaller R making orbit crossings more concentrated in R .

In Figure 7, we compare the mode structure (at otherwise similar properties) to the gravitational softening or disk thickness. At fixed ω and other disk properties, the modes in colder disks are higher- k (more tightly wound). This is also evident in the simulations in Hopkins & Quataert (2009) (see their Figures 2 & 4). This is because, for almost all the modes of interest, the mode has at least some contributions from the short-branch regime – they are analogous to the “p-modes” in Tremaine (2001), both in that the pressure/softening effects are non-negligible, in that the characteristic modes are trailing (the $kR > 0$ branch of the p-modes remains $kR > 0$ after refraction), and in that they have positive (prograde) pattern speeds. Because these modes depend on some non-zero β , as the modes themselves heat up the disk when they go non-linear (ultimately stabilizing it at some Q threshold), they can become more global. This has the effect (at fixed mode amplitude) of actually increasing the efficiency of the modes at driving large eccentricity and inflows to small radii, although the mode growth rates are lower. However, most of this difference depending on disk thickness is concentrated at small softening; once moderate disk thickness $\gtrsim 0.05 - 0.1$ is reached, the effect of the modes is actually fairly weakly dependent on the thickness.

Figure 8 compares the mode structure at fixed η and β but varying M_{disk} (and correspondingly a). At low $M_{\text{disk}}/M_{\text{BH}} \sim 0.1 - 0.3$, the first unstable modes to appear are, unsurprisingly, the maximally unstable modes with large $|kR| \approx 1/\beta$. As M_{disk} increases, the spectrum of unstable modes expands to include longer-wavelength modes, and by $M_{\text{disk}} \gtrsim M_{\text{BH}}$ includes very global modes. Once $M_{\text{disk}} \gg M_{\text{BH}}$, the structure at the radii we are interested in – i.e. in the quasi-Keplerian regime *inside* $\sim R_0$, is essentially independent of M_{disk} (it is identical to the case of an infinite power-law disk). Of course, there will in this limit be other modes at larger radii that are simply standard disk modes, but we are not interested in these behaviors.

5 COMPARISON WITH SIMULATIONS

Our analysis thus far is restricted to the linear regime. To see whether our key conclusions are robust in the non-linear regime, with gas+stellar systems (albeit still stellar-dominated), in the presence of inflow, star formation, feedback, and a non-trivial potential, we briefly compare to the mode structure in the simulations of self-consistently formed nuclear stellar disks from Hopkins & Quataert (2010c).

Figure 9 illustrates this in a typical nuclear scale simulation. We plot the enclosed disk $M_d(< R)$ and BH mass, mode pattern speed Ω_p (and circular speed Ω), and mode amplitudes, as a function of time in a system that is initially smooth (i.e. has no $m = 1$ perturbation). The mode first appears at some radii $\sim R_{\text{crit}}$, where $M_d/M_{\text{BH}} \sim 1$, with $\Omega_p \sim \Omega(R_{\text{crit}})$. At early times, the inner disk

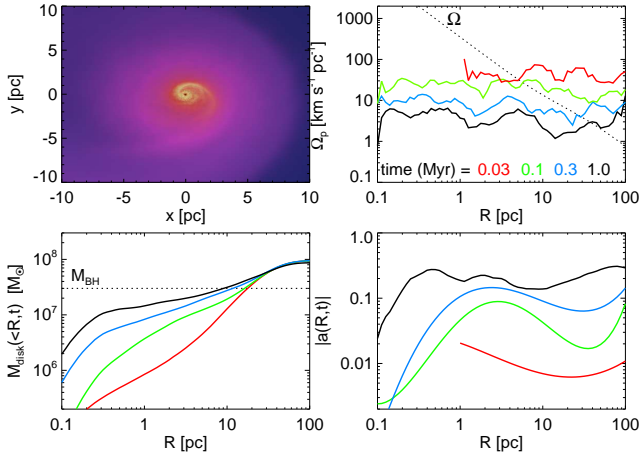


Figure 9. Nuclear mode origins, illustrated in a case study of a single, typical zoom-in simulation of nuclear scales showing the formation of the nuclear $m = 1$ mode that ultimately dominates accretion. *Top Left:* Image of the (saturated) mode. Brightness shows gas surface density, color (blue to yellow) encodes the specific SFR. *Top Right:* Best-fit mode pattern speed Ω_p (solid lines) in the simulation at each of several different times. Dotted line shows the circular velocity $\Omega(R)$. Modes are not plotted where they have no measurable amplitude. *Bottom Left:* Enclosed disk mass $M_d(<R)$, at the same times. Horizontal dotted line shows the BH mass. *Bottom Right:* Mode amplitude $|a|$ in the stellar disk. The mode originates where $M_d \sim M_{\text{BH}}$, as a locally fast mode ($\Omega_p \sim \Omega(R)$). It then propagates inwards, becoming a slow mode at smaller R . With time, the inflows generated move the inner instability radius inward, and the slowdown of the mode and change of mass profile shape (from those inflows) allow the mode to propagate to $r \rightarrow 0$, as shown. The stellar mode can be sustained for very long times, and at later times drives the gas mode (because stars dominate the mass).

profile is quite shallow (or even hollow), because no inflow has yet reached the center; we see the resulting cutoff in the range of the mode at small radius.

Two things work to push this range inwards. First, the mode slows down at early times, seen in Figure 9. This occurs both via angular momentum exchange with the bulge and disk at somewhat larger (~ 100 pc) radii (a resonant process not included in our analysis), and via direct carrying of some of the angular momentum in wavepackets in the gas after reflection off the inner radius above (through the OLR, apparent in the WKB treatment). This slowdown occurs while the system is in transition from the overstable growth phase to the nonlinear, quasi-steady state. It halts once the Ω_p is significantly below $\Omega(R_{\text{crit}})$; in these simulations the mode pattern speeds tend to stabilize at values $\sim 1 - 5 \text{ km s}^{-1} \text{ pc}^{-1}$. The process is analogous to the well-studied process of bar slowdown in unstable disks (although obviously with the bulge replacing the halo, which is dynamically irrelevant here), and we refer to those studies for further details (Weinberg 1985; Hernquist & Weinberg 1992; Athanassoula 2003; Martinez-Valpuesta et al. 2006), although there can be a non-trivial contribution to slowdown from the motion of the BH itself (damping via scattering off the background stars), an effect not included in analytic treatment (compare e.g. Adams et al. 1989; Shu et al. 1990). As Ω_p decreases, the barrier in Equation 19 likewise decreases, allowing the mode to strengthen and propagate inwards.

Second, the mode generates substantial gas inflows, which have three important effects. They lead to both gas mass available for further inflow, and form stars, which (discussed below) can sustain a long-lived mode at each radius. They directly move

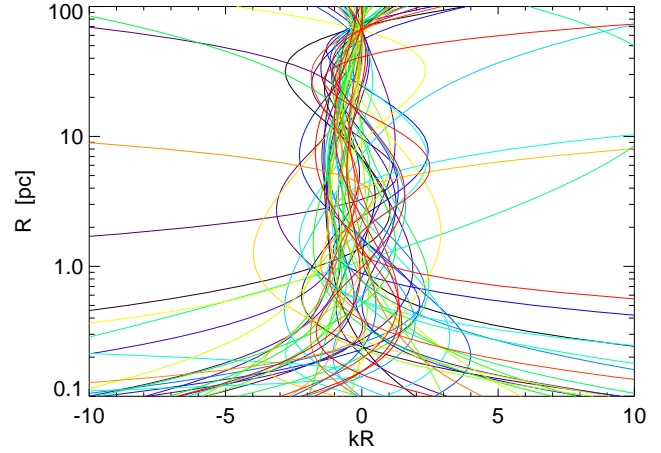


Figure 10. Nuclear mode structure. The radial wavenumber k versus radius R , fitted to modes at times near the peak of inflow for each of our nuclear-scale simulations. The modes are clearly global ($|kR| \sim 1$) at most radii. Some remain low- k to small R , but others wind up (although they can still propagate at finite k to $R \rightarrow 0$). Most wind up near ~ 100 pc, the effective OLR (but behavior here is complicated by interaction with the outer modes).

the $\tilde{f}_d \sim 0.1$ radius inwards, allowing the simple instability region to come closer to the BH. They also, correspondingly, steepen the surface density profile. Inflows will continuously increase the slope as long as inflow is “stalled” at any radius, and this is clearly reflected in Figure 9 as the enclosed disk mass at $R < R_{\text{crit}}$ rises rapidly with time. At this point, because of significant eccentricity at all radii, $v_r \sim V_c$ and $R_1 \sim R_0$, and orbit crossings can occur at all radii where the mode is supported. Thus, strong inflows can be sustained in systems such as that in Figure 9 down to radii where the BH completely dominates the potential.

The system quickly reaches a quasi-equilibrium state. The $m = 1$ mode has been excited down to $R = 0$; the mode pattern speeds stabilize and the mode amplitudes saturate. Figure 10 shows the structure of the modes, specifically the relation between R and kR , in different simulations at different times. For each simulation snapshot shown, we fit the density distribution over the radii plotted to an asymmetric $m = 1$ mode of the form $\Sigma_1 = |a(r)| \Sigma_0(r) \exp\{i(\int^r k(r) dr + \omega t - \phi)\}$, where Σ_0 is the aximuthally-averaged surface density and we allow $|a(r)|$ and $|k(r)|$ to vary as fifth-order polynomials in $\log(r)$ (the exact order makes little difference, though much higher order terms are noise-dominated). We then plot the instantaneous R and kR for each wave. Much of the behavior described above is evident: the modes are global $|kR| \sim 1$ at most radii – especially their origin – but many wind up at small $R \lesssim 1$ pc and large $R \gtrsim 100$ pc. We see both short and long branches appear in our simulations, but the short branch is more common – this appears to be set as a consequence of the “initial conditions” set by the earlier mode behavior, since in the earlier times while the mode moves to smaller R , it must wind up (given a shallow “pre-inflow” initial profile. At the largest radii, the real behavior is complicated by the interaction with the modes from the larger-scale inflows. At small radii, the behavior is anticipated by our arguments above.

6 DISCUSSION AND CONCLUSIONS

Lopsided or eccentric disk ($m = 1$) modes in quasi-Keplerian potentials are of considerable interest for a wide range of topics in astrophysics. Here, we have discussed how these modes originate in collisionless disks, with particular focus on the case of mostly stellar disks surrounding a supermassive BH. We discuss the origin, structural properties, propagation efficiencies, and resonance structure of such modes, comparing the simple analytic mode structure obtained from the WKB approximation, exact numerical solutions for the global linear mode structure in idealized disk+BH systems, and a full treatment of hydrodynamic simulations with gas+stars+BHs, star formation, and stellar feedback.

The solutions here clearly demonstrate that global, over-stable modes with linear growth rates $\gamma > 0$ are, in fact, normal modes of a BH-disk system and can propagate to $r \rightarrow 0$. In other words, our growing modes can be growing even at very small radii near the BH, where the enclosed disk mass is $\ll M_{\text{BH}}$ (here as low as $10^{-5} M_{\text{BH}}$). How can we reconcile this with the demonstration in Tremaine (2001) that slow modes in nearly-Keplerian disks are stable? The key is that the modes are *global*, and the disk is not *everywhere* quasi-Keplerian (nor is the mode everywhere a slow mode). If we enforce a cutoff to the disk mass profile or mode amplitude such that the regime of the mode is entirely inside a radius where $M_d(< R) \ll M_{\text{BH}}$, then we indeed recover these previous results and find that growing modes are not permitted. But if the disk extends to sufficiently large radii such that somewhere, $M_d(< R) \gtrsim (h/R) M_{\text{BH}}$ (the canonical self-gravity criterion), then at this radius instability is possible. And because the modes are global, the mode potential Φ_a at small radii $r \rightarrow 0$ can still have non-trivial contributions from radii where the mode is not slow and the potential is not Keplerian. As such, it is at least in principle possible to support growing modes at small radii.

Physically, the correct interpretation is that of the eccentricity propagating inwards, as discussed in § 3.2. In Tremaine (2001), it is noted that the non-axisymmetric potential Φ_a does not have to be self-generating; it can be imposed as some external Φ_e . The disk response at small radii is linear in Φ_e – thus, if it has some complex ω , so will the response. Here, the effective Φ_e is generated on large scales by the self-generating instability, where the disk is self-gravitating and the potential is only weakly Keplerian. The inner parts of the disk are stable according to the definition of Tremaine (2001); their behavior here is their linear response to the growing Φ_e imposed from where the disk is self-gravitating.

The $m = 1$ mode is special in this respect, in a quasi-Keplerian potential, because the system is near-resonance ($\Omega \approx \kappa$), so that the excited eccentricity at small radii is independent of the local ratio of disk to BH mass. All other (higher- m) modes may exist, but their propagation efficiencies and ability to induce large eccentricities (hence shocks, dissipation, and inflow) will be strongly suppressed by factors $\sim (M_d(< R)/M_{\text{BH}})$ at small radii.

Such modes appear as fast modes ($\Omega_p \sim \Omega(R_{\text{crit}})$) at the R_{crit} where the disk is moderately self-gravitating ($M_d(< R) \gtrsim (h/R) M_{\text{BH}}$ for local modes; for global modes, the criterion depends on the exact mass profile but is approximately $M_d(< R) \gtrsim 0.1 M_{\text{BH}}$). In this sense they are analogous to any unstable disk mode. The stellar waves are bounded by an OLR at a radius typically a factor \sim a couple in radius beyond co-rotation, although gaseous waves can move through this resonance. For this reason, growth rates of modes in pure fluid disks with a hard “edge” depend on reflection off that edge, and as such are quite sensitive to the boundary conditions (Shu et al. 1990; Ostriker et al. 1992; Nel-

son et al. 1998); but in gas+stellar systems or systems with a more smooth outer disk, the modes can refract and self-amplify without much dependence on the outer disk properties. If this represents the “first generation” of inflows, the inner disk profile may be shallow or hollow, so the mode may not be supported down to $r \rightarrow 0$ and will reflect off of a boundary at a factor of several smaller radii. But the mass profile will subsequently steepen owing to these inflows, until propagation to $R \rightarrow 0$ is possible.

Meanwhile, non-linear effects (seen in simulations) may have slowed down the pattern speed by a factor of a few. These include exchanges of angular momentum between the inner and outer disk/bulge/halo, and direct carrying of angular momentum in the induced gaseous waves (if present). The slowdown of the mode moves the OLR outwards and the inner radius inwards, and allows for more efficient propagation of the eccentricity and mass inflows. Once the critical slope is reached, and most of the gas mass has turned into stars, the mode reaches a quasi-equilibrium state. Since the stellar mode is fully bounded, and there is no buildup of mass at an intermediate radius, the pattern speed becomes nearly static, and the mass profile shape evolution slows down considerably. Large inflows are maintained to small R as long as gas is available, with a rate that scales roughly as $\dot{M}/\dot{M}_{\text{Edd}} \sim |a|$, the mode amplitude.

In terms of structural properties, the modes of interest are global, with $|kR| \lesssim$ a couple over most of their dynamic range (a factor of $> 10^4$ in radius. Indeed, in simulations, the modes seen are very global $|kR| \ll 1$ (essentially a pure elliptical/lopsided disk) over a significant dynamic range, but on sub-pc scales ($\sim 0.1 - 0.5$ pc), they can wind up into tighter spirals. Because they are low- k over most of the dynamic range, their structure is relatively insensitive to the coldness of the disk, for realistic values, and in extremely cold systems other effects will tend to heat the disks to moderate values quickly. And growing modes can be supported even in disks with large thickness $h/R \gtrsim 0.3$. In fact, as the thickness (or Q) increases, the mode growth rates do decrease, but most normal modes become more global, increasing their ability to pump up eccentricities and drive large inflow rates.

With sufficiently large mode amplitudes, there will be orbit crossings at many points around the elliptical orbit, but one is generally in the marginal orbit-crossing regime (in which there is ~ 1 orbit-crossing per orbit, near the axis of eccentricity). However, allowing for some gas in the disk with finite sound speed, the modes can easily drive shocks and dissipation at most radii where they have significant amplitude, even when there are no formal orbit crossings. The resulting inflow rates in this regime are treated in Hopkins & Quataert (2010a). Using the scalings therein, we estimate the inflow rates generated by these systems. For characteristic BH masses and radii of influence, these can be very large – corresponding to accretion at or near the BH Eddington limit, for moderate mode amplitudes $\gtrsim 0.1$. For plausible mass profile shapes in the “equilibrium” range, these shocks, dissipation, and inflow rates can be sustained down to extremely small radii $\sim 10^{-4} - 10^{-3} R_{\text{BH}}$, by which point the system has become a traditional viscous accretion disk. These modes therefore represent a viable and probably very important means of powering large accretion rates onto BHs, from $\sim 0.01 - 10$ pc scales.

Although we have usually considered the case of modes around a supermassive BH, our conclusions regarding collisionless disks may also be applicable in a number of non-galactic regimes. For example, a circum-stellar disk of planetesimals, or a system with a large density of planets. Comparing our results to those in Zakamska & Tremaine (2004), who study the efficiency of eccentric perturbation propagation in planetary systems, we find that

most of our conclusions still obtain despite the discrete nature of planetary systems, provided we take Σ to be the smeared-out (average) surface density profile. The mechanics of excitation and characteristic frequencies are similar, and they show that the efficiency of eccentricity propagation decreases for $\eta \gtrsim 1$, which we also find. If the mass in the collisionless (say, planetary) component of such disks is significant compared to the gas mass, and if the gaseous component can radiate efficiently when experiencing shocks, then our conclusions regarding inflow rates induced by these modes should be intact. Rescaling our predicted inflow rates to those appropriate for, say, a protostellar disk, they can be again quite large – $\sim 10^{-4} M_{\odot} \text{ yr}^{-1} (R[M_{\text{disk}} = M_{*}]/100 \text{ au})^{-3/2}$. Of course, our speculation regarding the role of star formation shaping these profiles on longer time scales should be modified appropriately (although there may be some analogies with planet formation in such disks). There may also be cases where proto-stellar disks experience eccentric perturbations from a collisionless component (say, induced modes from a binary companion or passages of neighboring stars/star-forming cores; see Krumholz et al. 2007), and these disks typically have mass ratios relative to the central object and power-law profiles in the mass range explicitly modeled here (Burrows et al. 1996; Hester et al. 1996). Exploring these applications in greater detail will be an important subject of future work.

ACKNOWLEDGMENTS

We thank Eliot Quataert and Scott Tremaine for helpful discussions in the development of this work. Support for PFH was provided by the Miller Institute for Basic Research in Science, University of California Berkeley.

REFERENCES

- Adams, F. C., Ruden, S. P., & Shu, F. H. 1989, *ApJ*, 347, 959
 Afanasiev, V. L., & Sil’chenko, O. K. 2002, *A&A*, 388, 461
 Athanassoula, E. 2003, *MNRAS*, 341, 1179
 Bate, M. R., Bonnell, I. A., & Price, N. M. 1995, *MNRAS*, 277, 362
 Binney, J., & Tremaine, S. 1987, *Galactic dynamics* (Princeton, NJ, Princeton University Press, 1987)
 Bornaud, F., Combes, F., Jog, C. J., & Puerari, I. 2005, *A&A*, 438, 507
 Burrows, C. J., et al. 1996, *ApJ*, 473, 437
 Christodoulou, D. M., & Narayan, R. 1992, *ApJ*, 388, 451
 Debattista, V. P., Ferreras, I., Pasquali, A., Seth, A., De Rijcke, S., & Morelli, L. 2006, *ApJL*, 651, L97
 Escala, A. 2007, *ApJ*, 671, 1264
 Gebhardt, K., et al. 1996, *AJ*, 112, 105
 Goldreich, P., & Tremaine, S. 1978, *ApJ*, 222, 850
 —. 1979, *ApJ*, 233, 857
 Hernquist, L., & Weinberg, M. D. 1992, *ApJ*, 400, 80
 Hester, J. J., et al. 1996, *AJ*, 111, 2349
 Hopkins, P. F., & Hernquist, L. 2010, *MNRAS*, 402, 985
 Hopkins, P. F., Murray, N., Quataert, E., & Thompson, T. A. 2010, *MNRAS*, 401, L19
 Hopkins, P. F., Murray, N., & Thompson, T. A. 2009, *MNRAS*, 398, 303
 Hopkins, P. F., & Quataert, E. 2009, *MNRAS*, in press, arXiv:0912.3257
 —. 2010a, *MNRAS*, in press, arXiv:1007.2647
 —. 2010b, *MNRAS*, in prep
 —. 2010c, *MNRAS*, 405, L41
 Houghton, R. C. W., Magorrian, J., Sarzi, M., Thatte, N., Davies, R. L., & Krajnović, D. 2006, *MNRAS*, 367, 2
 Jacobs, V., & Sellwood, J. A. 2001, *ApJL*, 555, L25
 Krumholz, M. R., Klein, R. I., & McKee, C. F. 2007, *ApJ*, 656, 959
 Lau, Y. Y., & Bertin, G. 1978, *ApJ*, 226, 508
 Lauer, T. R., et al. 1993, *AJ*, 106, 1436
 —. 1996, *ApJL*, 471, L79+
 —. 2005, *AJ*, 129, 2138
 Laughlin, G., & Bodenheimer, P. 1994, *ApJ*, 436, 335
 Laughlin, G., & Rozyczka, M. 1996, *ApJ*, 456, 279
 Levine, R., Gnedin, N. Y., Hamilton, A. J. S., & Kravtsov, A. V. 2008, *ApJ*, 678, 154
 Lin, C. C., Yuan, C., & Shu, F. H. 1969, *ApJ*, 155, 721
 Martinez-Valpuesta, I., Shlosman, I., & Heller, C. 2006, *ApJ*, 637, 214
 Mayer, L., Kazantzidis, S., Madau, P., Colpi, M., Quinn, T., & Wadsley, J. 2007, *Science*, 316, 1874
 Murray, C. D., & Dermott, S. F. 2000, *Solar System Dynamics*, Vol. ISBN 0521575974 (Cambridge, UK: Cambridge University Press)
 Nelson, A. F., Benz, W., Adams, F. C., & Arnett, D. 1998, *ApJ*, 502, 342
 Ostriker, E. C., Shu, F. H., & Adams, F. C. 1992, *ApJ*, 399, 192
 Papaloizou, J. C. B. 2002, *A&A*, 388, 615
 Salow, R. M., & Statler, T. S. 2001, *ApJL*, 551, L49
 Sambhus, N., & Sridhar, S. 2002, *A&A*, 388, 766
 Seth, A. C., et al. 2010, *ApJ*, in press, arXiv:1003.0680
 Shu, F. H., Tremaine, S., Adams, F. C., & Ruden, S. P. 1990, *ApJ*, 358, 495
 Thatte, N., Tecza, M., & Genzel, R. 2000, *A&A*, 364, L47
 Toomre, A. 1969, *ApJ*, 158, 899
 —. 1977, *ARA&A*, 15, 437
 Touma, J. R. 2002, *MNRAS*, 333, 583
 Tremaine, S. 2001, *AJ*, 121, 1776
 Weinberg, M. D. 1985, *MNRAS*, 213, 451
 Zakamska, N. L., & Tremaine, S. 2004, *AJ*, 128, 869